



# CO<sub>2</sub> Control Strategy for Large-Scale Cell Culture Bioreactor Operation

Naveenganesh Muralidharan<sup>\*</sup>, Thatsinee Johnson, Emma Bolduc, Mark Davis

Manufacturing Science and Technology (MSAT), AGC Biologics, Boulder, USA

## Email address:

nmural@agcbio.com (Naveenganesh Muralidharan)

<sup>\*</sup>Corresponding author

## To cite this article:

Naveenganesh Muralidharan, Thatsinee Johnson, Emma Bolduc, Mark Davis. (2024). CO<sub>2</sub> Control Strategy for Large-Scale Cell Culture Bioreactor Operation. *Advances in Bioscience and Bioengineering*, 12(1), 1-13. <https://doi.org/10.11648/abb.20241201.11>

**Received:** January 3, 2024; **Accepted:** January 17, 2024; **Published:** February 1, 2024

---

**Abstract:** In most mammalian cell culture operations, the pH is targeted to be close to neutral and the dissolved carbon dioxide [dCO<sub>2</sub>] concentration is desired to remain between 5 and 15% to avoid any inhibitory effects on cell growth. Typical cell culture scale-up approaches include maintaining constant power by volume (P/V) or a constant tip speed to set the impeller agitation rate or constant vvm to set the gas flow rate. However, these approaches are only focused on keeping the shear in the bioreactor system to a minimum and do not account for controlling the [dCO<sub>2</sub>] concentration within the desired range. Process engineers across industries have remediated the elevated [dCO<sub>2</sub>] concentration problem in large scale bioreactors by increasing gas flow rates; however, this approach is often trial and error. Therefore, in this article we review the current understanding of various factors that impact the dCO<sub>2</sub> concentration during the scale up of the cell culture process to large-scale bioreactors. This article also describes an easy and practical approach to predict and control the dCO<sub>2</sub> concentration in large-scale cell culture bioreactors using a mathematical predictive model developed based on mass-transfer first principles. We demonstrate the effective application and verification of the model by running a CHO cell culture process with a peak cell density of up to 20 x 10<sup>6</sup> Cells/mL in a 15,000 L bioreactor working volume.

**Keywords:** Bioreactor Scale Up, CO<sub>2</sub> Control, K<sub>La</sub>, Cell Culture CO<sub>2</sub> Concentration, CO<sub>2</sub> Predictive Model, CO<sub>2</sub> Bubble Saturation Time

---

## 1. Introduction

Elevated CO<sub>2</sub> concentrations have adverse impacts on cell health, causing changes in metabolic state, decreased cell productivity, and altering the glycosylation profile of therapeutic proteins [1]. Inhibitory effects on cell growth and productivity start at CO<sub>2</sub> concentrations 15% that of atmospheric pressure (760 mmHg), i. e., 115 mmHg [1]. Therefore, in biologics production, the CO<sub>2</sub> concentration in a cell culture bioreactor must be maintained below 115 mmHg. However, during scale up of bioreactor operations, maintaining the CO<sub>2</sub> profile below this maximum limit is considered challenging.

The simplest methodology that is most frequently used by process engineers to control CO<sub>2</sub> concentrations is manual feedback control. In this method, the dissolved CO<sub>2</sub> level in the cell culture liquid is measured, and if it exceeds a threshold

value (i.e., the action limit), the overall gas flow rate is increased by a certain amount [2]. However, a problem in manual feedback CO<sub>2</sub> control is identifying the correct increment for the total gas flow rate. This increment is often determined by trial-and-error, exposing the process to the risk of uncertainty. Accordingly, in the present study, we derived a sound mathematical model to predict and control the dissolved CO<sub>2</sub> concentration in a cell culture bioreactor as function of K<sub>La</sub>, pH set point, viable cell density, lactate, and the bicarbonate profile of the culture. The models have been verified in 15,000L bioreactor scale. This simplified model should help readers to predict and control CO<sub>2</sub> profiles in manufacturing-scale bioreactors easily. Furthermore, we discuss the current state of understanding on factors impacting excessive dissolved CO<sub>2</sub> accumulation in large-scale bioreactors in terms of geometrical bioreactor design and sparger configuration.

## 2. Impact of Excessive CO<sub>2</sub> Concentration to Cell Culture Performance

For a typical fed-batch cell culture, CO<sub>2</sub> is produced by cellular respiration as cells metabolize glucose, which plays a major role in energy production to support cell growth rate and productivity. Transport of polar and charged molecules like sugars and ions occurs through restrictive selective process in lipid bilayer membranes of the cells. However, uncharged molecules like CO<sub>2</sub> can freely diffuse through the lipid bilayer membrane. When excessive CO<sub>2</sub> enters the cytoplasm, it reacts with water to produce hydrogen ions, which changes the intracellular pH. This causes cells to spend energy on maintaining the pH rather than cell growth and protein

expression, as shown in Figure 1. In mammalian cell culture operation, cells consume glucose and produce lactate during exponential growth phase, later when the cells approach stationary phase cell switch the carbon consumption source from glucose to lactate, this metabolic switch in carbon source is defined Lactate metabolic shift (LMF). This LMF is desired in cell culture operation as it drives the process towards high titer yields and better quality on the protein. However, elevated CO<sub>2</sub> levels have been shown to delay or sometime inhibit the cells from undergoing desired lactate shift causing lactate accumulation in culture broth resulting in drop in pH leading to more base titrant addition by bioreactor's pH control. Increase in base titrant addition increases the osmolality, leading to inhibition of cell growth, thereby poor productivity, and variability in glycosylation profile in the therapeutic protein produced [3-6].

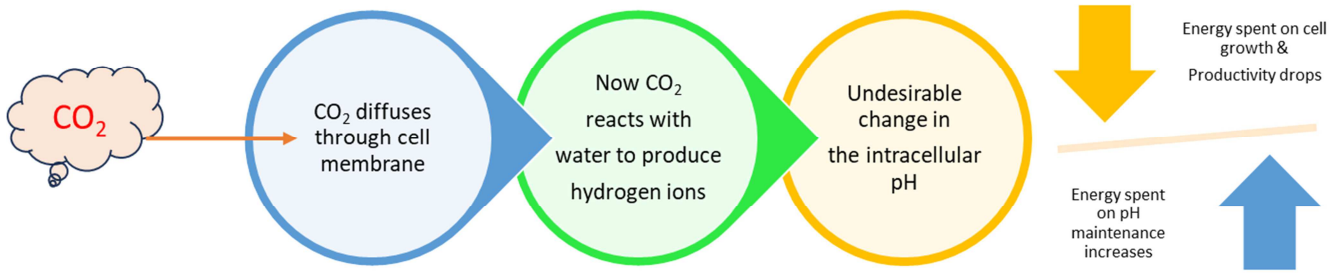


Figure 1. Impact of excessive CO<sub>2</sub> concentration on cell culture performance.

## 3. Factors Impacting Excessive CO<sub>2</sub> Accumulation

### 3.1. Effect of CO<sub>2</sub> Mass Transfer Coefficient

Early in the culture, it is necessary to sparge CO<sub>2</sub> to maintain the pH. However, as the cell density increases in the bioreactor, accumulation of CO<sub>2</sub> occurs due to cellular

respiration. For a typical cell culture process, for every mole of oxygen consumed, one mole of CO<sub>2</sub> is produced (Respiratory Quotient [RQ] = 1) [7]. Therefore, to maintain an optimal CO<sub>2</sub> concentration inside a bioreactor, oxygen transfer and CO<sub>2</sub> removal should be balanced. In other words, the O<sub>2</sub> transfer rate should be equal to the CO<sub>2</sub> transfer rate, as expressed in (1).

$$OTR = CTR \Rightarrow KLa_{O_2}(C_{B,O_2}^* - C_{L,O_2}) = -KLa_{CO_2}(C_{B,CO_2}^* - C_{L,CO_2}) \quad (1)$$

Here, KLa is the volumetric oxygen transfer coefficient, C<sub>B</sub><sup>\*</sup> and C<sub>L</sub> are the molar concentrations of O<sub>2</sub> or CO<sub>2</sub> in the purged gas bubble and liquid, respectively.

KLa is the product of KL (the film transfer coefficient) and a, i.e., the interfacial surface area per volume of the culture (m<sup>2</sup>/m<sup>3</sup>). Both CO<sub>2</sub> and O<sub>2</sub> experience the same interfacial surface area and hydrodynamic conditions inside the bioreactor, but KL differs for CO<sub>2</sub> and O<sub>2</sub>, and it is proportional to the liquid phase diffusivity of the respective gases, as shown in (2).

$$K_L = \sqrt{\frac{4 \cdot D_L \cdot \vartheta_B}{\pi \cdot d_B}} \quad (2)$$

Here, D<sub>L</sub> is the diffusivity,  $\vartheta_B$  is the bubble velocity, and d<sub>B</sub> is the bubble diameter. The diffusion constants for O<sub>2</sub> and CO<sub>2</sub> at 37°C are calculated as  $3.4 \times 10^{-9}$  and  $2.9 \times 10^{-9}$  m<sup>2</sup>/s, respectively, using Wilke and Chang's (1955) method, as shown in (3) [8].

$$D_L = \frac{1.173 \times 10^{-13} \times (A_{ss,M})^{0.5} \cdot T}{\mu \times V_m^{0.6}} \quad (3)$$

Applying the diffusivities of CO<sub>2</sub> and O<sub>2</sub> in (2), the mass transfer coefficient ratio of CO<sub>2</sub> to O<sub>2</sub> (Φ) is 0.90. This is in alignment with previously reported Φ values for large bubbles under laminar flow equal to 0.90. [9, 20].

Φ values below 0.90 have also been reported for micro spargers and at aggressively high gas flow rates using drilled hole spargers. The gas flow conditions for laminar flow can be assessed based on the bubble Reynolds number satisfying the condition of being less than 2000 (bubble Reynolds number is calculated per (8)) [10]. Reduced Φ values far below 0.90 at aggressive turbulent gas flow rates or while using micro spargers will reduce the CO<sub>2</sub> KLa in comparison to O<sub>2</sub> KLa and thereby increase excessive CO<sub>2</sub> accumulation. For gas flow rates to support up to  $20 \times 10^6$  cells/mL in our 15,000-L

bioreactor operating volume with sparger configuration ( $28 \times 1.6$  mm hole diameter), we satisfy the condition for laminar flow (i.e. Bubble Reynolds number  $< 2000$ ). Therefore, the assumption of  $\Phi = 0.90$  is valid for our bioreactor operating conditions. Readers must carefully evaluate their sparger configuration and bubble Reynolds number using (18) before assuming  $\Phi$  value of 0.90. It is also recommended to perform a separate  $K_La$  study specifically for  $CO_2$  when gas flow rate Reynolds numbers is  $> 2000$  and does not satisfy the conditions for laminar gas flow.

### 3.2. Effect of $CO_2$ Bubble Saturation Time

The changes in the concentrations of  $CO_2$  and  $O_2$  inside a gas bubble that is rising in a liquid column can be expressed as shown in (4) and (5) [12].

For changes in  $O_2$  concentration in a bubble:

$$\frac{dC_{O_2}}{dt} = m_{O_2} \cdot K_{G,O_2} \times \left(\frac{A_b}{V_b}\right) \times (C_{b,O_2} - C_{L,O_2}^*) \quad (4)$$

Here,

$$m_{O_2} = H_{O_2} \cdot R \cdot T$$

$$m_{O_2} = H_{O_2} \cdot R \cdot T; K_{G,O_2} = \left(\frac{D_{O_2}}{\delta}\right); V_b = \frac{4}{3} \pi r_b^3;$$

$$A_b = 4\pi r_b^2$$

$$\frac{dC_{CO_2}}{dt} = m_{CO_2} \cdot K_{G,CO_2} \times \left(\frac{A_b}{V_b}\right) \times (C_{L,CO_2}^* - C_{b,CO_2}) \quad (5)$$

Here,

$$m_{CO_2} = H_{CO_2} \cdot R \cdot T; K_{G,CO_2} = \left(\frac{D_{CO_2}}{\delta}\right)$$

Here;  $K_{G,O_2}$  and  $K_{G,CO_2}$  are the overall gas phase mass transfer coefficients for  $O_2$  and  $CO_2$  respectively,  $D_{O_2}$  and  $D_{CO_2}$  are the diffusion coefficients for  $O_2$  and  $CO_2$ , respectively,  $\delta$  is the thickness of the bubble film ( $\delta = 50 \mu m$  is a good approximation [17]),  $A_b$  is the surface area of a single bubble in  $m^2$ ,  $V_b$  is the volume of a single bubble in  $m^3$ ,  $C_b$  stands for the  $O_2$  or  $CO_2$  concentration of a bulk gas-phase bubble expressed in mmHg,  $C_L$  is the liquid phase concentration that is in equilibrium with the gas phase.  $m$  is defined as the partition constant. “ $m$ ” is the function of the solubility of a gas.  $CO_2$  and  $O_2$  have different solubilities in a fluid, as given by Henry’s coefficient expressed as the amount of gas that is solubilized per unit volume of the liquid per unit pressure in mmol/L.atm. The values of Henry’s coefficient ( $H$ ) are  $25 \times 10^{-3}$  and  $1 \times 10^{-3}$  mol/L.atm for  $CO_2$  and  $O_2$ , respectively. Therefore,  $CO_2$  is 25 times more soluble in liquid than oxygen in atmospheric pressure.

For illustration, assume a 0.5-mm-diameter air bubble is

rising in a liquid, and the size of the bubble remains constant with no shrinkage throughout its lifetime. Assuming air is purged through the sparger at atmospheric pressure (760 mmHg) and the mole fraction of  $O_2$  in air is 0.21, then the  $O_2$  concentration in the sparged air bubble is 159 mmHg ( $0.21 \times 760$  mmHg). For dissolved oxygen (DO), the set point of 40% is equal to 64 mmHg ( $0.40 \times 0.21 \times 760$  mmHg). Then the  $O_2$  and  $CO_2$  concentrations in the bubble at time zero are 159 and 0 mmHg, respectively, and the liquid  $O_2$  and  $CO_2$  concentrations are 64 and 115 mmHg, respectively. A sample calculation for changes in the  $O_2$  and  $CO_2$  concentrations in the bubble using (4) and (5) is shown in Figure 2A and 2B. Figure 2C shows the change in the concentration of  $O_2$  and  $CO_2$  in the bubble, demonstrating that the bubble attains 95% saturation for  $CO_2$  between 5 to 6 s. This value is in alignment with previously reported experimental values of between 5 and 9 s [3, 13]. Therefore, the driving force for  $CO_2$  drops to zero after 6 s and no further  $CO_2$  can be transferred into the bubble. On the other hand, for  $O_2$  transfer, bubble  $O_2$  concentration falls relatively slowly, and the bubble continues to supply  $O_2$  to the liquid as it rises. In comparison to  $O_2$ , as the bubble attains  $CO_2$  saturation in a short period, it is effective for  $CO_2$  removal only for a small portion of its lifetime. Figure 2D shows that rate of  $CO_2$  bubble saturation can be decreased by increasing the bubble diameter to improve  $CO_2$  removal rate.

### 3.3. Effect of Bioreactor Liquid Hydrostatic Pressure

Bioreactor aspect ratio, defined as liquid height to tank diameter ( $H_L/D_T$ ), is typically maintained between 1.0 to 1.5 [14, 15]. While scaling up the operational volume of the bioreactor, the liquid height increases per (6) and thereby increases the hydrostatic pressure  $P$  per (7). Fuller et al. (1966) developed an empirical correlation for diffusivity coefficient that shows an inverse relationship to pressure, as shown in (8) [16], (6) to (8) shows as bioreactor height increases thereby total pressure increases and diffusion coefficient decreases; making  $CO_2$  removal from a culture more challenging.

$$V_T = \frac{\pi \times D_T^2}{4} \times H_L; \text{Rearranging, } H_L = \left(\frac{4 \times V_T}{\pi \times 1.5^2}\right)^{1/3} \quad (6)$$

$$P_l = 1 \text{ atm} + \left[\rho_L \times g \times H_L \times \frac{(9.87e-6) \text{ atm}}{1 \text{ pascal}}\right] \quad (7)$$

Diffusivity as a function of pressure and temperature.

$$D_{A,B} = \frac{1.013 \times 10^{-7} \cdot T^{1.75} \left(\frac{1}{M_A} + \frac{1}{M_B}\right)^{1/2}}{P \left[v_A^{1/3} + v_B^{1/3}\right]^2} \quad (8)$$

Figure 3 shows the increase in the liquid height and corresponding solubility of  $CO_2$  for different bioreactor volumes with an assumed aspect ratio of 1.5.

	A	B	C	D	E	F	G
1	Change in the concentration of CO <sub>2</sub> in gas bubble				Change in the concentration of O <sub>2</sub> in gas bubble		
2	Diffusion coefficient, D, [m <sup>2</sup> /s]	2.87E-09			Diffusion coefficient, D, [m <sup>2</sup> /s]	3.40E-09	
3	Bubble diameter (mm)	0.5			Bubble diameter (mm)	0.5	
7	Bubble area, A <sub>b</sub> (m <sup>2</sup> )	7.85E-07			Bubble area, A <sub>b</sub> (m <sup>2</sup> )	7.85E-07	
8	Bubble volume, V <sub>b</sub> (m <sup>3</sup> )	6.54E-11			Bubble volume, V <sub>b</sub> (m <sup>3</sup> )	6.54E-11	
9	Bubble film thickness, δ (m)	5.00E-05			Bubble film thickness, δ (m)	5.00E-05	
10	K <sub>L</sub> (m/s) = D/δ	5.74E-05			K <sub>L</sub> (m/s) = D/δ	6.80E-05	
11	H, mol/L.Atm	2.50E-02			H, mol/L.Atm	1.07E-03	
12	Partition constant, m	0.64			Partition constant, m	0.03	
13	K <sub>G</sub> (A <sub>b</sub> /V <sub>b</sub> ), (1/s)	4.38E-01			K <sub>G</sub> (A <sub>b</sub> /V <sub>b</sub> ), (1/s)	2.22E-02	
14	Liquid dissolved CO <sub>2</sub> Conc; C <sub>L</sub> (mmHg)	115			Liquid dissolved O <sub>2</sub> Conc; C <sub>L</sub> (mmHg)	64	
15	Time (s)	ΔC = K <sub>G</sub> · (A <sub>b</sub> /V <sub>b</sub> ) · (C <sub>L</sub> - C <sub>b</sub> )	C <sub>b</sub> = ΔC <sub>n-1</sub> + C <sub>b(n-1)</sub>		Time (s)	ΔC = K <sub>G</sub> · (A <sub>b</sub> /V <sub>b</sub> ) · (C <sub>b</sub> - C <sub>L</sub> )	C <sub>b</sub> = C <sub>b(n-1)</sub> - ΔC <sub>n-1</sub>
16	0	50.4	0		0	2.1	159
17	1	28.3	50.4		1	2.1	156.9
18	2	15.9	78.7		2	2.0	154.8
19	3	8.9	94.6		3	2.0	152.8
20	4	5.0	103.6		4	1.9	150.8
21	5	2.8	108.6		5	1.9	148.9

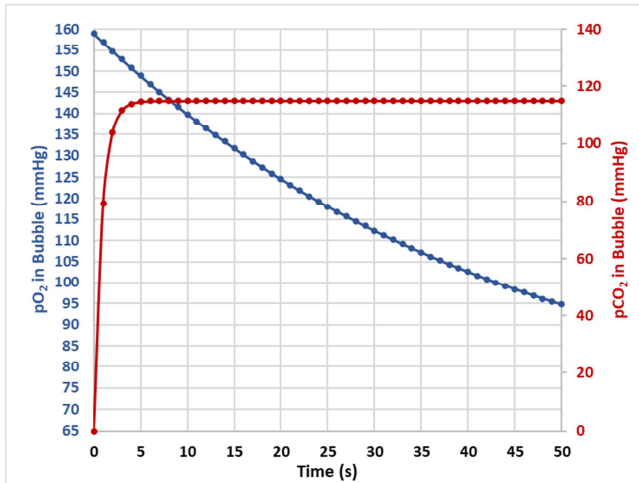
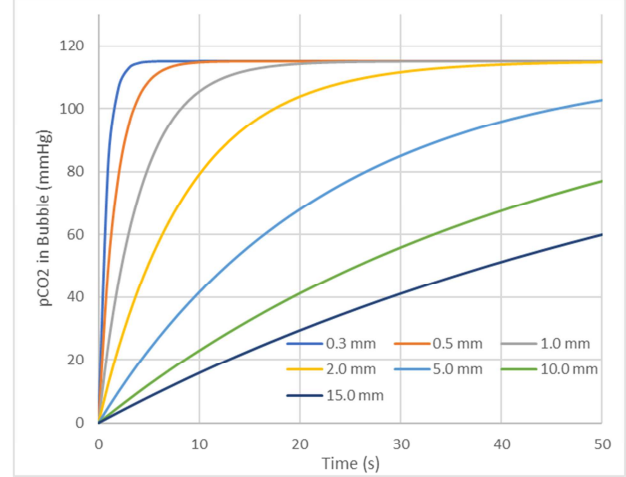
2A: Change in the concentration of O<sub>2</sub> in gas bubble calculation2B: Change in the concentration of CO<sub>2</sub> in gas bubble calculation2C: Bubble Saturation time for CO<sub>2</sub> and O<sub>2</sub> in a bubble with 0.5 mm diameter2D: Bubble Saturation time for CO<sub>2</sub> for different bubble diameters

Figure 2. Bubble saturation time.

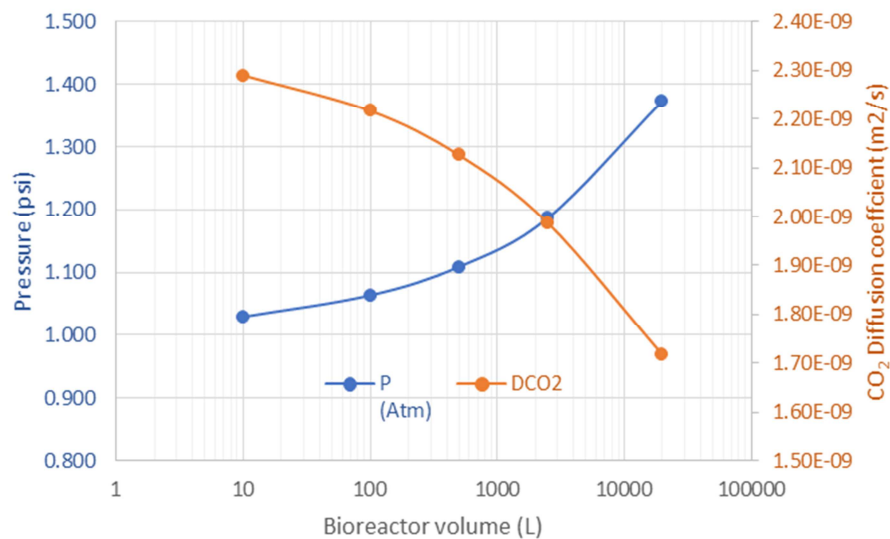


Figure 3. Impact of bioreactor height.

### 3.4. Effect of Difference in O<sub>2</sub> and CO<sub>2</sub> Driving Force

As the bubble germinates and rises through the liquid, the period of time from bubble generation to the bubble reaching the gas–liquid surface and disappearing is defined as bubble residence time ( $T_{B,R}$ ). During its lifetime in the liquid, a bubble serves two purposes for cell culture operation: 1) transferring O<sub>2</sub> from the bubble into the liquid, and 2) removing dissolved CO<sub>2</sub> from the liquid to the bubble. The rate of both O<sub>2</sub> transfer and CO<sub>2</sub> removal depends on driving force,  $\Delta C = C_s - C_T$ . Here,  $C_s$  and  $C_T$  are the starting and target concentrations of the gas species in the bubble.  $\Delta C$  dictates the driving force of gas mass transfer. For O<sub>2</sub> transfer: Assuming air is purged through the sparger at atmospheric, the O<sub>2</sub> concentration in the sparged air bubble  $C_{S,O_2}$  is 159 mmHg ( $0.21 \times 760$  mmHg). % DO set point ( $C_{T,O_2}$ ) of 40% is equal to 64 mmHg ( $0.40 \times 0.21 \times 760$  mmHg). The driving force for O<sub>2</sub> transfer is calculated to be 96 mmHg, as shown in (9) [1].

$$\Delta C_{O_2} = (C_{s,O_2} - C_{T,O_2}) = 96 \text{ mmHg} \quad (9)$$

For CO<sub>2</sub> transfer: The driving force for the CO<sub>2</sub> is expressed in (10).

$$\Delta C_{CO_2} = (C_{T,CO_2} - C_{Equil,CO_2}) \quad (10)$$

Here,  $C_{T,CO_2}$  is the desired maximum pCO<sub>2</sub> limit (115 mmHg) and  $C_{Equil,CO_2}$  is dissolved CO<sub>2</sub> concentration in equilibrium with the gas stream. To remove CO<sub>2</sub> from the

liquid at the same rate as the transfer of O<sub>2</sub> to the liquid, we need driving force  $\Delta C_{CO_2}$  equal to  $\Delta C_{O_2}$ . Hence equating (9) and (10) and solving for  $C_{Equil,CO_2}$  will yield a value of 19 mmHg, as expressed in (11).

$$C_{Equil,CO_2} = (115 - 96) \text{ mmHg} = 19 \text{ mmHg} \quad (11)$$

This value of 19 mmHg is only 2.5% of atmospheric pressure (760 mmHg). This means, as the bubble rises, when the CO<sub>2</sub> concentration in the bubble reaches 19 mmHg, the CO<sub>2</sub> removal rate drops below the O<sub>2</sub> transfer rate. Therefore, we define 19 mmHg as the rate-limiting maximum bubble CO<sub>2</sub> concentration,  $[C_{CO_2,RL}]$ , and time for the bubble to reach the maximum rate-limiting CO<sub>2</sub> concentration is defined as the bubble CO<sub>2</sub> rate-limiting equilibrium time  $T_{B,RL}$ . If the bubble residence time  $T_{BR}$  is less than  $T_{B,RL}$ , then the bubble is efficient in removing CO<sub>2</sub> throughout its lifetime. If  $T_{BR}$  is larger than  $T_{B,RL}$ , then the bubble is efficient in CO<sub>2</sub> removal equivalent to O<sub>2</sub> transfer only until time  $T_{B,RL}$ . Hence, larger fast rising bubbles with shorter residence times are more efficient than smaller bubbles with longer residence times [1, 7].

For a typical cell culture bioreactor process, O<sub>2</sub> KLa is enhanced by using micro spargers and/or a blend of pure O<sub>2</sub> and air to increase the driving force  $\Delta C$ . Both lead to sufficient O<sub>2</sub> transfer rates using low gas flow rates, which further enhances the accumulation of CO<sub>2</sub> at the large scale.

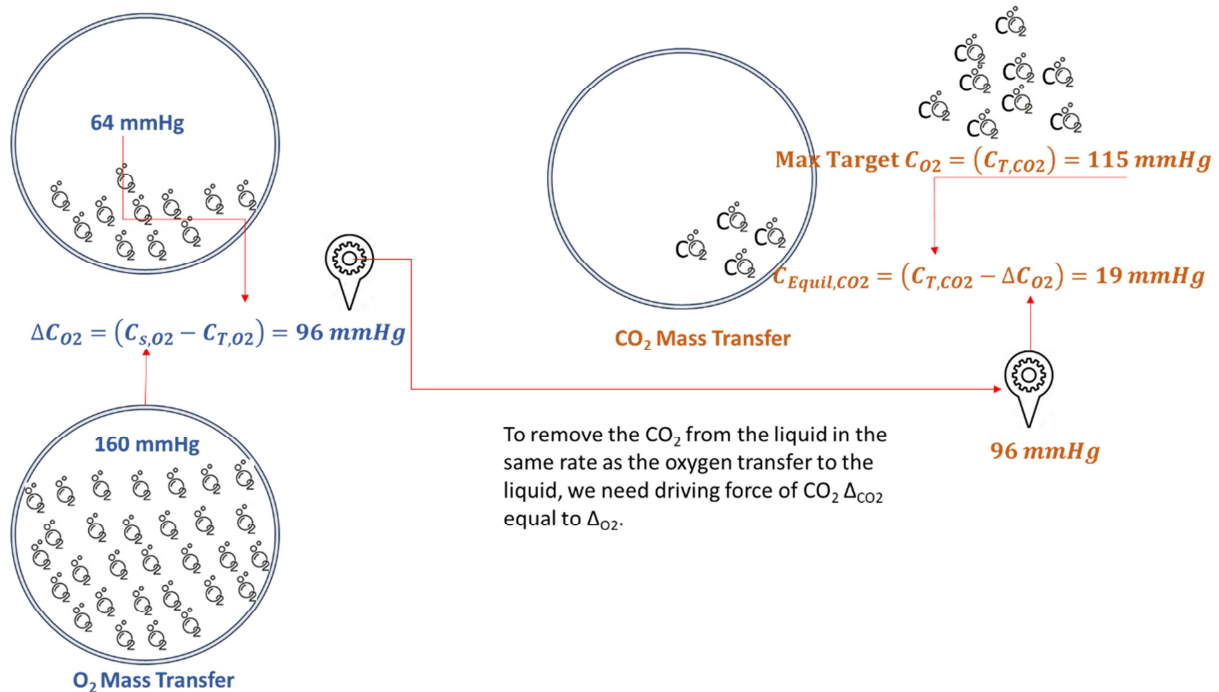


Figure 4. Difference in O<sub>2</sub> and CO<sub>2</sub> driving forces on excessive CO<sub>2</sub> accumulation.

### 3.5. Effect of Sparger Design and Gas Entrance Velocity

As discussed before, bubble residence time plays a critical role in the dissolved CO<sub>2</sub> concentration in a culture broth. The

faster the bubble travels through the liquid column, the more efficient is the CO<sub>2</sub> transfer rate. The bubble velocity is a function of bubble size. The bubble size and bubble velocity can be calculated using (12) to (17) [17, 18].



$$GEV = \frac{Q_g}{n_O \left( \frac{\pi d_b^2}{4} \right)} \quad (12)$$

$$d_b = 1.17 \cdot GEV^{0.4} \cdot d_o^{0.8} \cdot g^{0.2} \quad (13)$$

$$V_1 = \frac{1}{36} \times \frac{(\rho_L - \rho_g) \cdot g \cdot d_b^2}{\mu_L} \quad (14)$$

$$V_2 = V_1 \left[ 1 + 0.73667 \frac{(g \cdot d_b)^{1/2}}{V_1} \right]^{1/2} \quad (15)$$

$$V_3 = \left( \frac{3 \cdot \sigma}{\rho_L \cdot d_b} + \frac{g \cdot d_b \cdot (\rho_L - \rho_g)}{2 \cdot \rho_L} \right)^{1/2} \quad (16)$$

$$\vartheta_b = 1 \div \sqrt{\frac{1}{V_2^2} + \frac{1}{V_3^2}} \quad (17)$$

$$N_{Bubble, Re} = \frac{d_o \cdot GEV \cdot \rho}{\mu} \quad (18)$$

Figure 5 shows the bubble rise velocity as a function of bubble diameter. Bubbles with sizes less than 0.1 mm (or 100  $\mu$ m), called microbubbles, have low rising velocities. Here, the bubble movement is dominated by liquid surface tension leading to reduced bubble rising velocity, causing longer bubble residency time in the bioreactor and poor CO<sub>2</sub> removal from the cell culture. Smaller bubbles give higher mass transfer areas, but also have slow rising velocities and reduced CO<sub>2</sub> driving force. Therefore, the optimum operating conditions for effective CO<sub>2</sub> removal is a sparger flow rate that maintains the ratio of bubble residence time to bubble saturation time  $\geq 1.0$ .

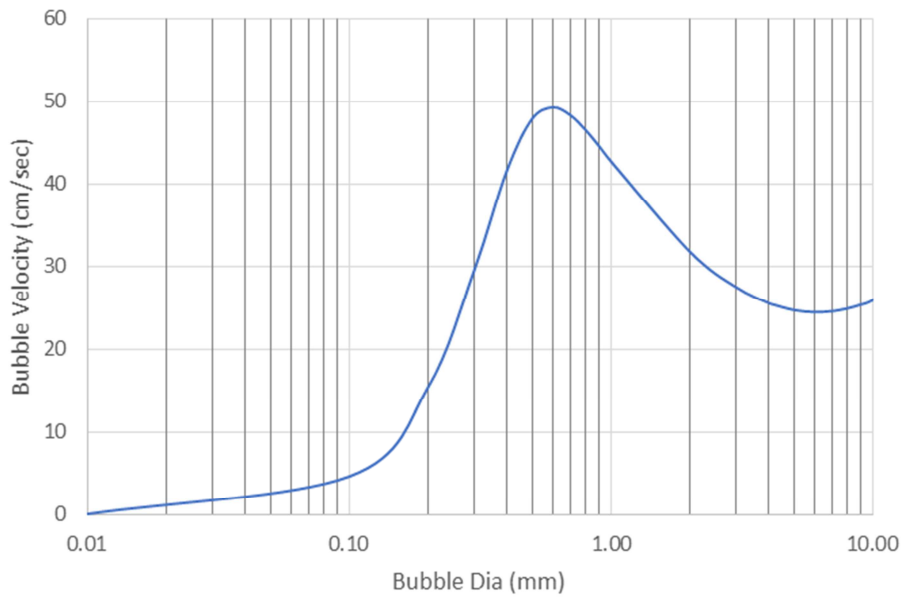


Figure 5. Bubble diameter vs. bubble rise velocity.

## 4. CO<sub>2</sub> Predictive Model Assumptions and Limitations

### 4.1. Assumptions

1. The rate of mass transfer is much faster than the O<sub>2</sub> uptake rate and CO<sub>2</sub> evolution rate of cells. Therefore, the mass balance governing equations; O<sub>2</sub> transfer rate equals O<sub>2</sub> uptake rate, and CO<sub>2</sub> transfer rate equals CO<sub>2</sub> evolution rate.
2. The bioreactor mass transfer system is assumed to be at a pseudo-steady state. This means over the very short period of bubble residence time in the bioreactor, the O<sub>2</sub> and CO<sub>2</sub> concentration in the liquid is not changing while the CO<sub>2</sub> concentration in bubbles is dynamic and changing continuously.
3. The cell culture performance attributes, like viable cell density, oxygen uptake rate, lactate profile, and bicarbonate profile, are known from previous at-scale or

small-scale runs.

4. This model also assumes the biological metabolite consumption and production rate of cells is conserved across different scales of bioreactor operation and from batch to batch.
5. The sparge rate is sufficiently low to prevent bubble coalescence.
6. As the bubbles rise through the liquid, the drop in O<sub>2</sub> mole fraction from the bubbles is compensated by increase in CO<sub>2</sub> mole fraction in the bubbles.

### 4.2. Limitations

1. This model can only be used when the bioreactor mass transfer co-efficient (*K<sub>La</sub>*) is characterized.
2. The model assumes that the *K<sub>La</sub>* from surface gas-liquid interface is small and insignificant compared to the mass transfer from sparging gas bubbles, and is therefore applicable only for large manufacturing-scale bioreactors.
3. The assumption that CO<sub>2</sub> *K<sub>La</sub>* = 0.90 times O<sub>2</sub> *K<sub>La</sub>* is

applicable only for bubbles generated under laminar conditions using drilled hole spargers and does not apply to bubbles generated using micro spargers or when gas flow rates using drilled hole spargers are operated under turbulent conditions.

4. This model only accounts for major metabolites like CO<sub>2</sub>, lactate, and bicarbonate for pH control that are most frequently measured in cell culture process. Therefore, it does not include other organic acids or base components produced by cells during fermentation.

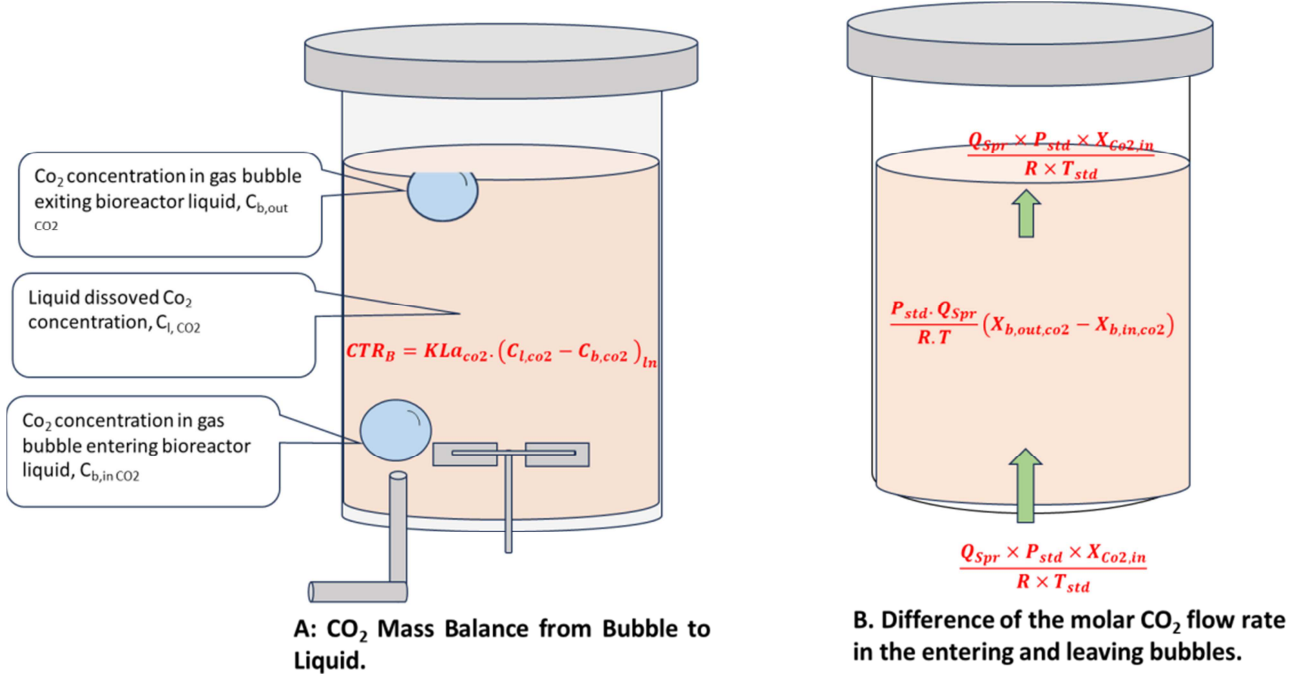


Figure 6. CO<sub>2</sub> Mass balance for the gas transfer in bioreactor system.

#### 4.3. CO<sub>2</sub> Predictive Model Development

As shown in Figure 6A, the CO<sub>2</sub> transfer rate from the liquid to sparged gas bubbles can be expressed as shown in (19). Here  $C_{b,CO_2}$  represents the CO<sub>2</sub> concentration in the bubble (mmol/L),  $C_{l,CO_2}$  represents the liquid dissolved CO<sub>2</sub> concentration (mmol/L), and  $KLa_{CO_2}$  represents the CO<sub>2</sub> mass transfer coefficient (1/h). The suffix (ln) indicates logarithmic mean for driving force. In large-scale bioreactors, because of the gradient of increasing hydrostatic pressure from the surface of the liquid to the bottom of the vessel, the composition of a gas phase bubble is dynamic. Accordingly, the driving force is expressed as logarithmic mean driving force [11].

$$CTR_B \cdot V = KLa_{CO_2} \cdot V \cdot (C_{l,CO_2} - C_{b,CO_2})_{ln} \quad (19)$$

The logarithmic mean gas bubble CO<sub>2</sub> concentration can be expressed as the function of bubble CO<sub>2</sub> concentration entering and leaving the culture liquid in the bioreactor, as shown in (20) [11]. Here, the suffixes  $b_{in,CO_2}$  and  $b_{out,CO_2}$

indicate CO<sub>2</sub> concentration in bubble going into the liquid and exiting the liquid, respectively.

$$(C_{l,CO_2} - C_{b,CO_2})_{ln} = \frac{(C_{b,in,CO_2} - C_{b,out,CO_2})}{\ln\left(\frac{C_{l,CO_2} - C_{b,in,CO_2}}{C_{l,CO_2} - C_{b,out,CO_2}}\right)} \quad (20)$$

Substituting (20) in (19) gives (21):

$$CTR_B \cdot V = KLa_{b,CO_2} \left( \frac{(C_{b,in,CO_2} - C_{b,out,CO_2})}{\ln\left(\frac{C_{l,CO_2} - C_{b,in,CO_2}}{C_{l,CO_2} - C_{b,out,CO_2}}\right)} \right) \cdot V \quad (21)$$

The dissolved CO<sub>2</sub> concentration in equilibrium with the gas stream in (21) can be expressed as a function of Henry's constant, system pressure, and mole fraction of CO<sub>2</sub>, (Concentration,  $C = P \cdot H \cdot X$ ) by applying Henry's law, as shown in (22) [11]. Here,  $P_i$  is pressure (atm),  $H$  is the Henry coefficient (mol/L.atm), and  $X$  is the mole fraction of gas. Suffixes  $b_{in,CO_2}$  and  $b_{out,CO_2}$  represent CO<sub>2</sub> concentration in a bubble going into the liquid and exiting the liquid, respectively.

$$CTR_B \cdot V = KLa_{b,CO_2} \cdot V \left( \frac{(X_{b,out,CO_2} \cdot P_{l,CO_2} \cdot H_{CO_2} - X_{b,in,CO_2} \cdot P_{l,CO_2} \cdot H_{CO_2})}{\ln\left(\frac{C_{l,CO_2} - C_{b,in,CO_2}}{C_{l,CO_2} - C_{b,out,CO_2}}\right)} \right) \quad (22)$$

As shown in Figure 6B, the moles of CO<sub>2</sub> transferred from the sparge stream can also be determined from the difference

of the molar CO<sub>2</sub> flow rate in the entering and leaving bubbles. If we assume that the gas hold-up volume is constant, then the

CO<sub>2</sub> transfer rate from the sparger can be expressed as shown in (23). Here  $P_{std}$  is the standard pressure (Atm),  $Q_{spr}$  represents sparger flow rate,  $R$  is the relative gas constant, and  $T$  is the temperature in K.

$$CTR_B \cdot V = \frac{P_{std} \cdot Q_{spr}}{R \cdot T} (X_{b,out,CO_2} - X_{b,in,CO_2}) \quad (23)$$

Now equating (22) and (23), will yield (24)

$$KLa_{b,CO_2} \cdot V \left( \frac{(X_{b,out,CO_2} - X_{b,in,CO_2}) P_{l,CO_2}}{\ln \left( \frac{C_{l,CO_2} - C_{b,in,CO_2}}{C_{l,CO_2} - C_{b,out,CO_2}} \right)} \right) = \frac{P_{std} \cdot Q_{spr}}{R \cdot T} (X_{b,out,CO_2} - X_{b,in,CO_2}) \quad (24)$$

Simplification of (24) will yield (25).

$$\ln \left( \frac{C_{l,CO_2} - C_{b,in,CO_2}}{C_{l,CO_2} - C_{b,out,CO_2}} \right) = \frac{KLa_{b,CO_2} \cdot V \cdot R \cdot T \cdot P_{l,CO_2}}{P_{std} \cdot Q_{spr}} \quad (25)$$

For simplification in further calculation, the right-hand side of (25) is termed as a constant named  $A_{CO_2}$ , as this term has no unit all together.

$$\frac{KLa_{b,CO_2} \cdot V \cdot R \cdot T \cdot P_{l,CO_2}}{P_{std} \cdot Q_{spr}} = A_{CO_2} \quad (26)$$

Substituting (25) in (26)

$$\left( \frac{C_{l,CO_2} - C_{b,in,CO_2}}{C_{l,CO_2} - C_{b,out,CO_2}} \right) = \text{Exp}(A_{CO_2}) \quad (27)$$

Re-arranging the numerator and denominator in (27), the right-hand side of the (27)  $\text{Exp}(A_{CO_2})$  takes a negative sign as

$$X_{b,out,CO_2} \cdot P_{l,CO_2} = C_{l,CO_2} (1 - \text{Exp}(-A_{CO_2})) + X_{b,in,CO_2} \cdot P_{l,CO_2} \cdot \text{Exp}(-A_{CO_2}) \quad (30)$$

Now substituting (26) and (30) in (22) and solving for dissolved  $C_{l,CO_2}$  will yield (31) to predict the liquid dissolved CO<sub>2</sub> concentration. Refer to Appendix A for details of algebraic mathematical simplification.

$$C_{l,CO_2} = \frac{CTR_T \cdot A_{CO_2} + KLa_{b,CO_2} \cdot X_{b,in,CO_2} \cdot P_{l,CO_2} \cdot (1 - \text{Exp}(-A_{CO_2}))}{KLa_{b,CO_2} (1 - \text{Exp}(-A_{CO_2}))} \quad (31)$$

Often In cell culture bioreactor operation, liquid dissolved CO<sub>2</sub> is measured as partial pressure of CO<sub>2</sub> (pCO<sub>2</sub>) in millimetre mercury (mmHg). The CO<sub>2</sub> concentration calculated using Equation 32 is converted to pCO<sub>2</sub> in mmHg using the ideal gas law ( $P \times V = n \times R \times T$ ). Rearranging the ideal gas expression will yield dissolved pCO<sub>2</sub> as follows: Here,  $T$  is temperature expressed in Kelvin.

$$pCO_2 = C_{l,CO_2} \times R \times T \quad (32)$$

In (31), there are two unknown terms: CO<sub>2</sub> transfer rate (CTR) and mole fraction of CO<sub>2</sub> ( $X_{b,in,CO_2}$ ). CO<sub>2</sub> transfer rate can be calculated from CO<sub>2</sub> evolution rate (CER), which in turn is dependent on oxygen uptake rate (OUR) of the cells and respiratory quotient (RQ). CER is calculated as shown in (33). Here RQ is defined as the moles of CO<sub>2</sub> released for every mole of O<sub>2</sub> consumed. Hu (2020) reported a RQ value of 1.0 for mammalian cells [7].

$$CTR = CER = RQ \cdot OUR \quad (33)$$

*Mole Fraction of CO<sub>2</sub> ( $X_{b,in,CO_2}$ ) from Medium Chemistry*

Typical cell culture media buffering is achieved using a CO<sub>2</sub>-bicarbonate based buffer. The pH of the medium is

shown in (28).

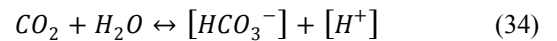
$$\left( \frac{C_{l,CO_2} - C_{b,out,CO_2}}{C_{l,CO_2} - C_{b,in,CO_2}} \right) = \text{Exp}(-A_{CO_2}) \quad (28)$$

Expressing dissolved CO<sub>2</sub> concentration in equilibrium with the gas stream in (28), as a function of Henry's constant, system pressure and mole fraction of CO<sub>2</sub>, (Concentration,  $C = P \cdot H \cdot X$ ) by the Applying Henry's law will yield (29). [6, 8].

$$\left( \frac{C_{l,CO_2} - X_{b,out,CO_2} \cdot P_{l,CO_2}}{C_{l,CO_2} - X_{b,in,CO_2} \cdot P_{l,CO_2}} \right) = \text{Exp}(-A_{CO_2}) \quad (29)$$

Rearranging (29) and solving for concentration of CO<sub>2</sub> in bubble exiting the liquid is given by (30):

dependent on the fine balance of dissolved carbon dioxide (CO<sub>2</sub>) and bicarbonate (HCO<sub>3</sub><sup>-</sup>). Often, cell culture carbonate buffered media is operated around neutral pH. CO<sub>2</sub> reacts with water to form carbonic acid, as shown in (34) [19].



Assuming the amount of dissolved CO<sub>2</sub> in the culture medium is equal to the amount of CO<sub>2</sub> in gas phase at equilibrium and applying the Henderson–Hasselbalch principle, the cell culture medium buffer can be expressed as shown in (35) [19].

$$pH = pKa + \frac{[HCO_3^-]}{[CO_2]} \quad (35)$$

In mammalian cell culture fermentation, one other metabolite lactate plays a critical role in medium buffer chemistry. Lactate is a predominant metabolite produced by cells that brings the pH into the acidic range in bioreactor environments. Lactate has an equilibrium constant pKa of 5.5. Because a typical cell culture is maintained around neutral pH 7.0, one mole of lactate produced by cells will demand one mole of base titrant for neutralization. Due to this neutralization, the culture broth now displaces the acidic component of the buffer in the form of CO<sub>2</sub> gas. So, the effective concentration of base in the culture will be  $[HCO_3^-] - [\text{Lactate}]$  [19]. Based on this reaction in the culture, we can now introduce lactate into the Henderson–Hasselbalch equation, and Equation (35) can be rewritten as shown in (36).



$$pH = pKa + \frac{[HCO_3] - [Lactate]}{[CO_2]} \quad (36)$$

Gramer et al. (2007) showed an empirical relationship between pH, CO<sub>2</sub>, lactate, and bicarbonate concentration, as shown in (37), and verified the application of the model in (37) using actual cell culture runs [19].

$$[Lac] = [HCO_3] - 0.88 \cdot [CO_2\%]^{0.79} \cdot 10^{(pH-6.38)} \quad (37)$$

Here, lactate and bicarbonate concentrations are expressed in mmol/L, CO<sub>2</sub> concentration is expressed in %.

Based on the correlation expression shown in (37), a contour

plot was created showing the lactate concentration in g/L as a function of pCO<sub>2</sub> in (%) and bicarbonate concentration in mMol for four different pH values ranging from 6.90 to 7.05 typically used for cell culture, as shown in Figure 7. The mole fraction of CO<sub>2</sub> in the gas purge can be calculated based on the cell culture lactate and bicarbonate concentrations. In some cell culture platform process, post inoculation rather than calling CO<sub>2</sub> under pH control, CO<sub>2</sub> is sparged between 5 to 10% for a specific short period of time between 24 to 48 hours to ensure specific amount of CO<sub>2</sub> is maintained in the culture, in such instances mole fraction sparged CO<sub>2</sub> gas is substituted for the value of X<sub>b,in,CO2</sub> instead of using Figure 7.

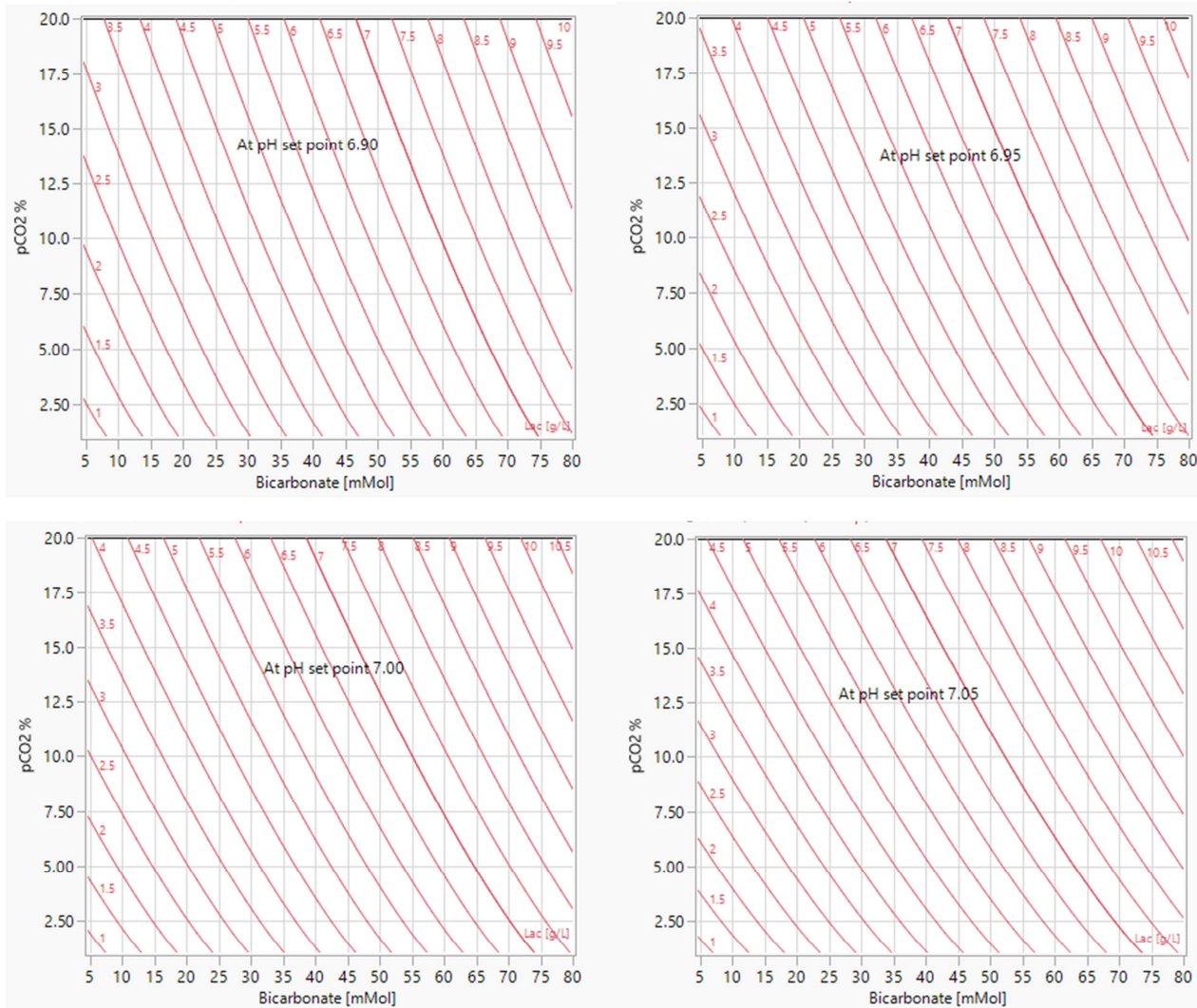


Figure 7. Correlation between pH, pCO<sub>2</sub>, lactate, and bicarbonate to determine the mole fraction of CO<sub>2</sub> (X<sub>b,inCO2</sub>).

## 5. At Scale Model Verification and Successful Implication of Predictive Model

We ran a high cell density CHO cell culture process up to 20 × 10<sup>6</sup> cell/mL peak cell density in 15,000L bioreactor working volume. The pCO<sub>2</sub> concentration was measured using Nova

Flex 2 metabolite analyzer. Twenty-three actual measured pCO<sub>2</sub> values are plotted against the predicted values as shown in Figure 8A, linear regression of predicted over measured CO<sub>2</sub> values gave an R<sup>2</sup> = 0.87 demonstrates, that the predictive expression is reliable. Additionally, the p-value less than 0.001 demonstrates the measure of strength of association between the predicted and actual values is statistically significant. Figure 8B shows Density Ellipse fit. The density ellipse shows the degree of correlation between the predictive and

explanatory variable using correlation coefficient and its p value. The correlation coefficient shown in Figure 8C is the Pearson correlation coefficient ( $r$ ) and it is the most common way of measuring a linear correlation. It is a number ranging between  $-1$  and  $1$  that measures the strength and direction of the linear relationship between two variables.  $r = 0.93$  demonstrates, that there is a linear relationship between predicted and actual pCO<sub>2</sub> values is strong and p value of  $<0.0001$  for regression coefficient “ $r$ ” signifies that the linear relationship is statistically significant. Figure 8C shows the residual plot at different measured actual CO<sub>2</sub> concentration.

Figure 8C, demonstrates for 19 out of 23 data points the absolute difference between the measured and predicted CO<sub>2</sub> values are within  $\pm 10$  mmHg which is the expected range for QC level-1 standard check with the mean pCO<sub>2</sub> value of 70 mmHg for NovaFlex2 metabolite analyzer. Furthermore, as the measurement range increases, the acceptable expected range also increases that explains the higher residual values at measured pCO<sub>2</sub> above 100 mmHg. NovaFlex2 analyzer used for this study does not have any QC standard checks above 70 mmHg.

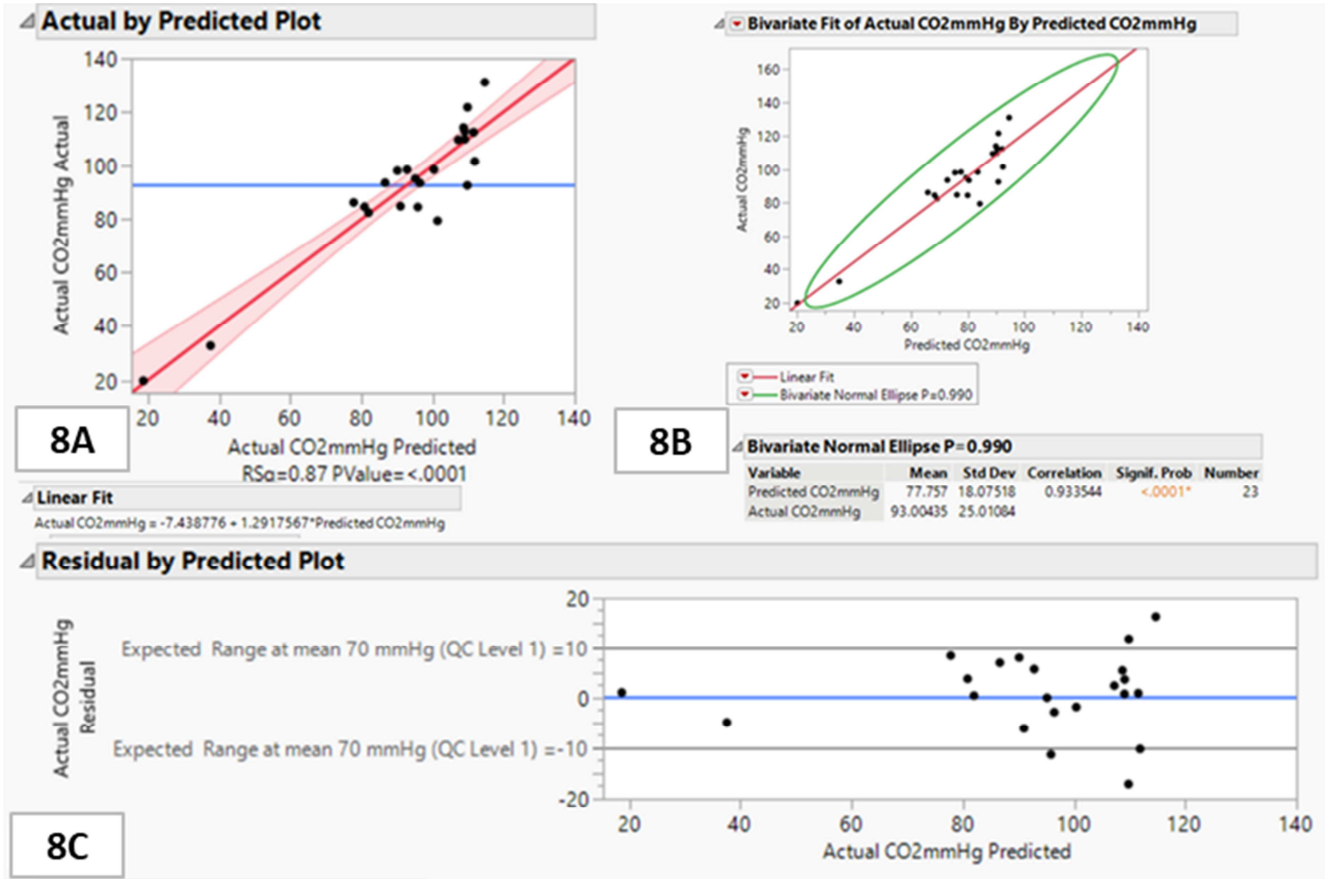


Figure 8. pCO<sub>2</sub> predictive model validation.

## 6. Sample Design Space for Bioreactor Operation to Control pCO<sub>2</sub>

A contour plot was drawn to predict the dissolved CO<sub>2</sub> concentration using (31) with sparger total gas flow rate and viable cell density as explanatory variables, as shown in Figure 9. The assumptions for the parameters in the predictive model are summarized in Table 1, based on the values reported by Hu (2022), to represent typical production bioreactor operating conditions [1, 7].

Additionally, Equation (31) demands two more input values, that is CO<sub>2</sub> mole fraction and K<sub>La</sub>. For CO<sub>2</sub> mole fraction, Figure 7 is used with the assumptions in Box 1; A CO<sub>2</sub> mole

fraction of 5% is calculated. 4 to 7% is a good approximation to cover a wide range of cell culture operation. For K<sub>La</sub> value, a predictive expression created by experimental studies is used, as reported in our previous published article Muralidharan et al. (2024) [17]. Based on the above assumptions, a contour profile was created showing pCO<sub>2</sub> profile as a function of gas flow rate and viable cell density, as shown in Figure 9.

Table 1. pCO<sub>2</sub> Predictive Model Assumptions.

Henry Coefficient H = 25 mmol/L. Atm
Temperature 37°C
pH set point = 7.00
Bicarbonate concentration = 35 mmol/L
Lactate concentration = 4.0 g/L.
Bioreactor Volume = 15,000 L
Impeller Agitation Rate = 30 RPM

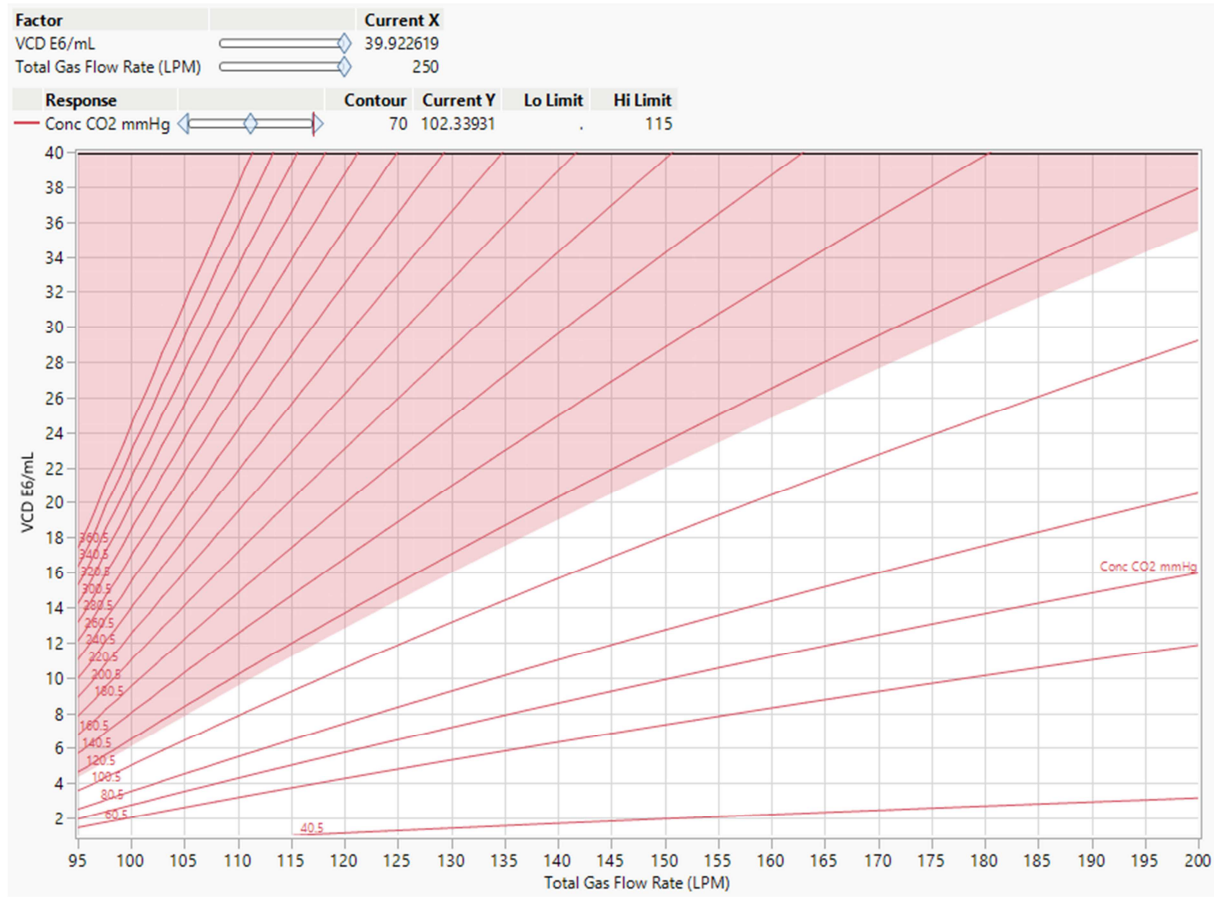


Figure 9.  $p\text{CO}_2$ , design space for bioreactor operating conditions.

## 7. Conclusions

This article summarizes the impact of excessive  $\text{CO}_2$  accumulation in cell culture operation, considering factors in scaling up that cause the  $\text{CO}_2$  accumulation. A predictive model to predict and control  $\text{CO}_2$  accumulation in large manufacturing-scale bioreactors is presented. Readers are encouraged to carefully weigh the limitations of this model to assess its suitability before applying it to their systems. As shown in Figure 8, there is an offset between the predicted to actual  $p\text{CO}_2$  value. This could be due to variability of measurement instrument and the limitations of the assumptions in the model. However, the application of this model is to estimate the increment in total gas flow rate required to control excessive  $\text{CO}_2$  accumulation.

## Abbreviations

$A_{ss}$ : Association factor for the solvent (-). 2.6 for water.  
 $C$ : Molar concentrations of gas in purged gas or liquid. (mmol/L or mmHg).  
 $\text{CTR}$ : Carbon dioxide Transfer Rate (mmol/L.hr)  
 $d_B$ : Bubble diameter (m)  
 $d_o$ : Sparger hole / orifice diameter (m)  
 $D$ : Diffusion Coefficient ( $\text{m}^2/\text{s}$ )

$D_T$ : Diameter of the tank (m)  
 $g$ : Specific gravity 9.8 ( $\text{m/s}^2$ )  
 $\text{GEV}$ : Gas entrance velocity (m/s)  
 $H_L$ : Liquid height in the tank (m)  
 $H_{\text{O}_2}$  and  $H_{\text{CO}_2}$ : Henry's coefficient (H) is  $25 \times 10^{-3}$  and  $1.07 \times 10^{-3}$  mol/L.atm for  $\text{CO}_2$  and  $\text{O}_2$ , respectively.  
 $K_L$ : Film transfer coefficient (m/s)  
 $\text{KLa}$ : Overall mass transfer coefficient for  $\text{O}_2$  and  $\text{CO}_2$  (1/hr).  
 $M$ ,  $M_A$  and  $M_B$ : Molecular weights of the solute and solvent in g/mol ( $M_{\text{CO}_2} = 44$ ,  $M_{\text{O}_2} = 32$ ,  $M_{\text{H}_2\text{O}} = 18$ ).  
 $m_{\text{O}_2}$  and  $m_{\text{CO}_2}$ : Partition coefficient is 0.64 and 0.03 (-) for  $\text{CO}_2$  and  $\text{O}_2$ , respectively.  
 $\text{OTR}$ : Oxygen Transfer Rate (mmol/L.hr)  
 $P_t$ : Total pressure in the system (Atm)  
 $Q_g$ : Volumetric sparger gas flow rate ( $\text{m}^3/\text{s}$ )  
 $R$ : Relative gas constant,  $8.21 \times 10^{-5}$  L/Atm/mmol.K  
 $r_b$ : Bubble radius (m)  
 $T$ : Temperature (K)  
 $V_m$ : Molecular volume of the solute at its boiling point = 0.034 and 0.025  $\text{m}^3/\text{Kmol}$  for  $\text{CO}_2$  and  $\text{O}_2$ , respectively.  
 $V_T$ : Volume of the tank ( $\text{m}^3$ )  
 $v_A$  and  $v_B$ : Diffusion volume coefficients of the solute and solvent ( $v_{\text{CO}_2} = 26.9$ ,  $v_{\text{O}_2} = 16.6$ ,  $v_{\text{H}_2\text{O}} = 10.73$ ).  
 $\rho_L$  and  $\rho_g$ : Dynamic density of the liquid and gas, respectively ( $\text{Kg/m}^3$ )

$\sigma$ : Surface tension of the solution  
 $\mu$  or  $\mu_L$ : Viscosity of the solution (0.66 mNs/m<sup>2</sup> for cell culture medium is good approximation)

0009-0006-9259-5284 (Thatsinee Johnson)  
 0009-0009-2162-6284 (Emma Bolduc)  
 0009-0000-3759-7486 (Mark Davis)

## ORCID

0009-0002-3884-3217 (Naveenganesh Muralidharan)

## Conflicts of Interest

The authors declare no conflicts of interest.

## Appendix

*Appendix A1. Algebraic mathematical simplification from Equation 30 to Equation 31.*

Step-1	$CTR_T = KLa_{b,co2} \cdot \left( \frac{(C_{l,co2}(1 - \text{Exp}(-A_{co2})) + X_{b,in,co2} \cdot P_l \cdot H_{co2} \cdot \text{Exp}(-A_{co2}) - X_{b,in,co2} \cdot P_l \cdot H_{co2})}{A_{co2}} \right)$
Step-2	$CTR_T = KLa_{b,co2} \cdot \left( \frac{(C_{l,co2}(1 - \text{Exp}(-A_{co2})) + X_{b,in,co2} \cdot P_l \cdot H_{co2} \cdot (\text{Exp}(-A_{co2}) - 1))}{A_{co2}} \right)$
Step-3	$CTR_T = KLa_{b,co2} \cdot \left( \frac{(C_{l,co2}(1 - \text{Exp}(-A_{co2})) - X_{b,in,co2} \cdot P_l \cdot H_{co2} \cdot (1 - \text{Exp}(-A_{co2})))}{A_{co2}} \right)$
Step-4	$CTR_T = KLa_{b,co2} \cdot \left( \frac{(C_{l,co2}(1 - \text{Exp}(-A_{co2})) - X_{b,in,co2} \cdot P_l \cdot H_{co2} \cdot (1 - \text{Exp}(-A_{co2})))}{A_{co2}} \right)$
Step-5	$CTR_T \cdot A_{co2} = KLa_{b,co2} \cdot ((C_{l,co2}(1 - \text{Exp}(-A_{co2})) - X_{b,in,co2} \cdot P_l \cdot H_{co2} \cdot (1 - \text{Exp}(-A_{co2}))))$
Step-6	$CTR_T \cdot A_{co2} = (KLa_{b,co2} \cdot C_{l,co2}(1 - \text{Exp}(-A_{co2})) - (KLa_{b,co2} \cdot X_{b,in,co2} \cdot P_l \cdot H_{co2} \cdot (1 - \text{Exp}(-A_{co2}))))$
Step-7	$CTR_T \cdot A_{co2} + KLa_{b,co2} \cdot X_{b,in,co2} \cdot P_l \cdot H_{co2} \cdot (1 - \text{Exp}(-A_{co2})) = (KLa_{b,co2} \cdot C_{l,co2}(1 - \text{Exp}(-A_{co2})))$
Step-8	$CTR_T \cdot A_{co2} + KLa_{b,co2} \cdot X_{b,in,co2} \cdot P_l \cdot H_{co2} \cdot (1 - \text{Exp}(-A_{co2})) = KLa_{b,co2} \cdot C_{l,co2} - KLa_{b,co2} \cdot C_{l,co2} \cdot \text{Exp}(-A_{co2})$
Step-9	$CTR_T \cdot A_{co2} + KLa_{b,co2} \cdot X_{b,in,co2} \cdot P_l \cdot H_{co2} \cdot (1 - \text{Exp}(-A_{co2})) = C_{l,co2} (KLa_{b,co2} - KLa_{b,co2} \cdot \text{Exp}(-A_{co2}))$
Step-10	$\frac{CTR_T \cdot A_{co2} + KLa_{b,co2} \cdot X_{b,in,co2} \cdot P_l \cdot H_{co2} \cdot (1 - \text{Exp}(-A_{co2}))}{(KLa_{b,co2} - KLa_{b,co2} \cdot \text{Exp}(-A_{co2}))} = C_{l,co2}$
Step-11	$C_{l,co2} = \frac{CTR_T \cdot A_{co2} + KLa_{b,co2} \cdot X_{b,in,co2} \cdot P_l \cdot H_{co2} \cdot (1 - \text{Exp}(-A_{co2}))}{KLa_{b,co2}(1 - \text{Exp}(-A_{co2}))}$

## References

- [1] Hu, W. "SCALING UP AND SCALING DOWN ON CELL CULTURE BIOREACTORS." In Cell Culture Bioprocess Engineering, 2nd ed., 281. CRC Press, 2020.
- [2] Muralidharan, N., Johnson, T., & Davis, M. (2023, November 16). Identifying False Metabolite Measurements During Cell-Culture Monitoring Effective Application of the Multivariate Hotelling's T2 Statistic. Bioprocess International, 21(11-12), 29-31. Retrieved from <https://bioprocessintl.com/2023/november-december-2023/identifying-false-metabolite-measurements-during-cell-culture-monitoring-effective-application-of-the-multivariate-hotellings-t2-statistic/>
- [3] Xing, Z., Lewis, A. M., Borys, M. C., & Li, Z. J. (2017). A carbon dioxide stripping model for mammalian cell culture in manufacturing scale bioreactors. Biotechnology and Bioengineering, 114(6), 1184-1194. <https://doi.org/10.1002/bit.26232>
- [4] DeZengotita, V. M., Schmelzer, A. E., & Miller, W. M. (2002). Characterization of hybridoma cell responses to elevated pCO<sub>2</sub> and osmolality: Intracellular pH, cell size, apoptosis, and metabolism. Biotechnology and Bioengineering, 77(4), 369-380. <https://doi.org/10.1002/bit.10176>
- [5] Mostafa, S. S., & Gu, X. (2003). Strategies for improved dCO<sub>2</sub> removal in large - scale fed - batch cultures. Biotechnology Progress, 19(1), 45-51. <https://doi.org/10.1021/bp0256263>
- [6] Xing, Z., Kenty, B. M., Li, Z. J., & Lee, S. S. (2009). Scale - up analysis for a CHO cell culture process in large - scale bioreactors. Biotechnology and Bioengineering, 103(4), 733-746. <https://doi.org/10.1002/bit.22287>
- [7] Hu, W. "OXYGEN TRANSFER IN CELL CULTURE BIOREACTORS." In Cell Culture Bioprocess Engineering, 2nd ed., 219. CRC Press, 2020.
- [8] Wilke, C. R., & Chang, P. (1955). Correlation of diffusion coefficients in dilute solutions. AIChE Journal, 1(2), 264-270. <https://doi.org/10.1002/aic.690010222>
- [9] Royce, P. N., & Thornhill, N. F. (1991). Estimation of dissolved carbon dioxide concentrations in aerobic fermentations. AIChE Journal, 37(11), 1680-1686. <https://doi.org/10.1002/aic.690371111>
- [10] Muralidharan, N. (2023, February 9). Shear-Proof Design Space: Scaling Stirred-Tank Bioreactors for Cell Culture Processes. Bioprocess International, 21(1-2), 36-38. <https://bioprocessintl.com/upstream-processing/bioreactors/shear-proof-design-space-scaling-stirred-tank-bioreactors-for-cell-culture-processes/>
- [11] Doran, P. M. (1995). Mass Transfer. In Bioprocess Engineering Principles (1st ed., p. 210- 213). Elsevier Science & Technology Books.
- [12] Katoh, S., Horiuchi, J., & Yoshida, F. (2015). Mass Transfer. In Biochemical engineering: A textbook for engineers, chemists and biologists (2nd ed., p. 73- 77). John Wiley & Sons.
- [13] Sieblist, C., Hägeholz, O., Aehle, M., Jenzsch, M., Pohlscheidt, M., & Lübbert, A. (2011). Insights into large - scale cell - culture reactors: II. gas - phase mixing and CO<sub>2</sub> stripping. Biotechnology Journal, 6(12), 1547-1556. <https://doi.org/10.1002/biot.201100153>
- [14] Liow, K. Y., Thouas, G. A., Tan, B. T., Thompson, M. C., & Hourigan, K. (2009). Modelling the transport of momentum and oxygen in an aerial-disk driven bioreactor used for animal tissue or cell culture. IFMBE Proceedings, 1672-1675. [https://doi.org/10.1007/978-3-540-92841-6\\_415](https://doi.org/10.1007/978-3-540-92841-6_415)

- [15] Stadler, E. L., & B. Braun Biotech Inc. (2001, October). Fermentor / Bioreactor Design Lecture [Paper presentation]. Bioprocess Equipment Design Seminar, Atlanta, GA.
- [16] Fuller, E. N., Schettler, P. D., & Giddings, J. C. (1966). New method for prediction of binary gas-phase diffusion coefficients. *Industrial & Engineering Chemistry*, 58(5), 18-27. <https://doi.org/10.1021/ie50677a007>
- [17] Muralidharan, N., Bolduc, E., & Davis, M. (2024, January/February). Characterizing Oxygen Mass Transfer and Shear During Cell Culture Calculating the Maximum Cell Density Supported By a 20,000-Liter Stirred-Tank Bioreactor. *Bioprocess International*, 22(1-2).
- [18] Baz-Rodríguez, S., Aguilar-Corona, A., & Soria, A. (2012). RISING VELOCITY FOR SINGLE BUBBLES IN PURE LIQUIDS. *Revista Mexicana de Ingeniería Química*, 11(2), 269-278. <https://www.scielo.org.mx/pdf/rmiq/v11n2/v11n2a6.pdf>
- [19] Gramer, M. J., & Ogorzalek, T. (2007). A semi - empirical mathematical model useful for describing the relationship between carbon dioxide, pH, lactate and base in a bicarbonate - buffered cell - culture process. *Biotechnology and Applied Biochemistry*, 47(4), 197-204. <https://doi.org/10.1042/ba20070001>
- [20] Calderbank, P., & Moo-Young, M. (1961). The continuous phase heat and mass-transfer properties of dispersions. *Chemical Engineering Science*, 16(1-2), 39-54. [https://doi.org/10.1016/0009-2509\(61\)87005-x](https://doi.org/10.1016/0009-2509(61)87005-x)